Oversaturating Liquid Interfaces with Nanoparticle-Surfactants

Xuefei Wu[,1], Han Xue[*,1], Zachary Fink[1,2], Brett A. Helms[1,3], Paul D. Ashby[3], Ahmad K. Omar[1,4], Thomas P. Russell[†,1,2,5]*

[1]Materials Sciences Division, Lawrence Berkeley National Laboratory, Berkeley, CA 94720, USA
[2]Polymer Science and Engineering Department, University of Massachusetts, Amherst, MA 01003, USA
[3]Molecular Foundry, Lawrence Berkeley National Laboratory, Berkeley, CA 94720, USA
[4]Department of Materials Science and Engineering, University of California, Berkeley, Berkeley, CA 94720, USA
[5]Advanced Institute for Materials Research (AIMR), Tohoku University, 2-1-1 Katahira, Aoba, Sendai 980-8577, Japan
Email: russell@mail.pse.umass.edu

Abstract

Assemblies of nanoparticles (NPs) at liquid interfaces hold promise as dynamic "active" systems when there are convenient methods to drive the system out of equilibrium via crowding. To this end, we show that oversaturated assemblies of charged NPs can be realized and held in that state with an external electric field. Upon removal of the field, strong interparticle repulsive forces cause a high in-plane electrostatic pressure that is released in an explosive emulsification. We quantify the packing of the assembly as it is driven into the oversaturated state under an applied electric field. Physiochemical conditions substantially affect the intensity of the induced explosive emulsification, underscoring the crucial role of interparticle electrostatic repulsion.

Keywords: out-of-equilibrium assembly • nanoparticle-surfactants • *in-situ* small-angle X-ray scattering • explosive emulsification • liquid/liquid interface

Introduction

Out-of-equilibrium self-assembled structures underpin many "active" systems that mimic living systems[1-4]. Many intricate structures and functions within living organisms are a result of non-equilibrium assemblies on length scales ranging from the molecular to cellular levels[5-7]. However, unlike self-assembled systems at equilibrium, where thermodynamic variables dictate the packing and saturation conditions, out-of-equilibrium assemblies can be kinetically trapped in states or structures well-below or well-above the

equilibrium saturation point.

Out-of-equilibrium self-assembled structures can be generated through the use of an external field. The field may be in the form of a time-varying temperature, or the use of an applied field, e.g., an electric [8-11]/magnetic[12-14] field, light[3, 15, 16], chemical fuel[17], or fluid flow[18-20], that forces a non-equilibrium packing of the assembly. Depending on the components comprising the assembly, the spatial arrangements of the components in the non-equilibrium assembly can impart properties or functions far different from the assembly at equilibrium. Subsequent to the removal of the field, the system attempts to relax to the equilibrium state, but how rapidly this relaxation occurs will be system- and condition-dependent. If non-equilibrium assemblies are vitrified or jammed[21, 22], relaxation is markedly slowed or arrested. If non-equilibrium assemblies are ordered or there are strong interparticle interactions[3], relaxations can also be exceedingly slow.

To realize the out-of-equilibrium assemblies at the interface, one needs to first control the adsorption of NPs to the immiscible liquid/liquid interface and prevent aggregation-induced irreversible close packing. Diffusion-driven[23] and ethanol-induced[24-26] adsorption to the liquid interface are among the most widely used strategies. Spontaneous self-assembly is the most convenient method, however, this approach has often led to inhomogeneous ordering of NPs as well as the appearance of void areas with low area coverage ratio[23]. Here, we exploits the electrostatic interactions between the charged NPs dispersed in the aqueous phase and surfactants dissolved in the other liquid phase, along with complementary counterions forming the nanoparticle-surfactants (NPSs)[21, 22], it has been discovered that NPs can create a densely packed 2D film at the liquid/liquid interface[27]. This arrangement allows for the adjustment of interparticle interactions by modulating the electrostatic forces between them simply through the addition of electrolytes[28], pH adjustments[29, 30], or concentration changes[31]. This method is readily accessible to achieve dense packed NPs assemblies at the liquid/liquid interface and does not depend on the incorporation of low-dielectric solvents. Therefore, in this manuscript, we adopted this method to facilitate the spontaneous adsorption of NPs at a water/oil interface.

When NPs are oversaturated at an interface due to the application of an external field, their stability post-field removal is influenced by their binding energy to the interface and their interactions with each other. Usually, NPs have a low binding energy, leading to their ejection from the interface to alleviate stress[32]. Previous studies have reported that voltage-tunable charged NPs array at liquid/liquid interface could create an electro-tunable quasi-two-dimensional plasmonic platform by adjusting its packing density at the interface.[32-34] The application of an electric field can either drive these charged NPs toward the interface or pull them away, dependent on the orientation of the field. At the interface, a potential energy well compels the NPs to overcome electrostatic repulsion among themselves, thereby elevating their

reversible packing density. However, by attaching ligands to form NPSs, this binding energy increases, preventing ejection and arresting the system in a jammed non-equilibrium state.[21, 22, 35] If the NPSs are charged, the strong interparticle electrostatic repulsion leads to explosive emulsification after rapid field removal[36]. Here, the rapid ejection of hundreds of thousands of charged microdroplets decorated with a jammed layer of NPSs, forms a charged plume that propels the parent droplet by electrostatic forces, turning it into an "active droplet"[37].

To better understand the behavior of NPS assemblies, it is important to link their macroscopic behavior to nanoscopic structure. Due to the small size of NPs, the available experimental techniques for *in-situ* investigation of assemblies at liquid/liquid interfaces are limited. Liquid cell transmission electron microscopy offers one method, but it is hindered by the requirement of thin liquid layers and difficulties in applying a field[38]. Open cell scanning electron microscopy can detail NP or NPS assemblies on a surface, but cannot easily access a liquid/liquid interface[39, 40]. The Surface enhanced Raman scattering (SERS) signal of the molecules near the gold NPs (Au NPs) allows for the detection and identification of molecular species at very low concentrations[41, 42], but it is limited to only detect a target with Raman signals[43-45]. UV-vis measurement can extract NP spatial information through localized plasmon coupling between the NPs, yet its sensitivity diminishes at greater interparticle distances[46-48]. *In-situ* grazing incidence small-angle X-ray scattering, however, is ideally suited to characterize the in-plane and out-of-plane packing of NPS assembled at a fluid-fluid interface.[27, 49-53]

Here, *in-situ* X-ray scattering is used to elucidate the NPS packing microstructure at a water/toluene interface under an applied electric field in real time (Fig. 1(a)). The distance between NPSs is found to decrease with external electric field intensity as the NPS packing densifies until oversaturation. The balance between electrostatic repulsion between NPSs at the interface and their response to the applied field determines the level of oversaturation and the intensity of the explosive emulsification realized after field removal. Increasing ligand concentration intensifies this emulsification, especially under alkaline conditions. However, if ligand concentration surpasses a threshold, oversaturation of the NPSs cannot be achieved and only spontaneous emulsification is found.

Results and Discussions

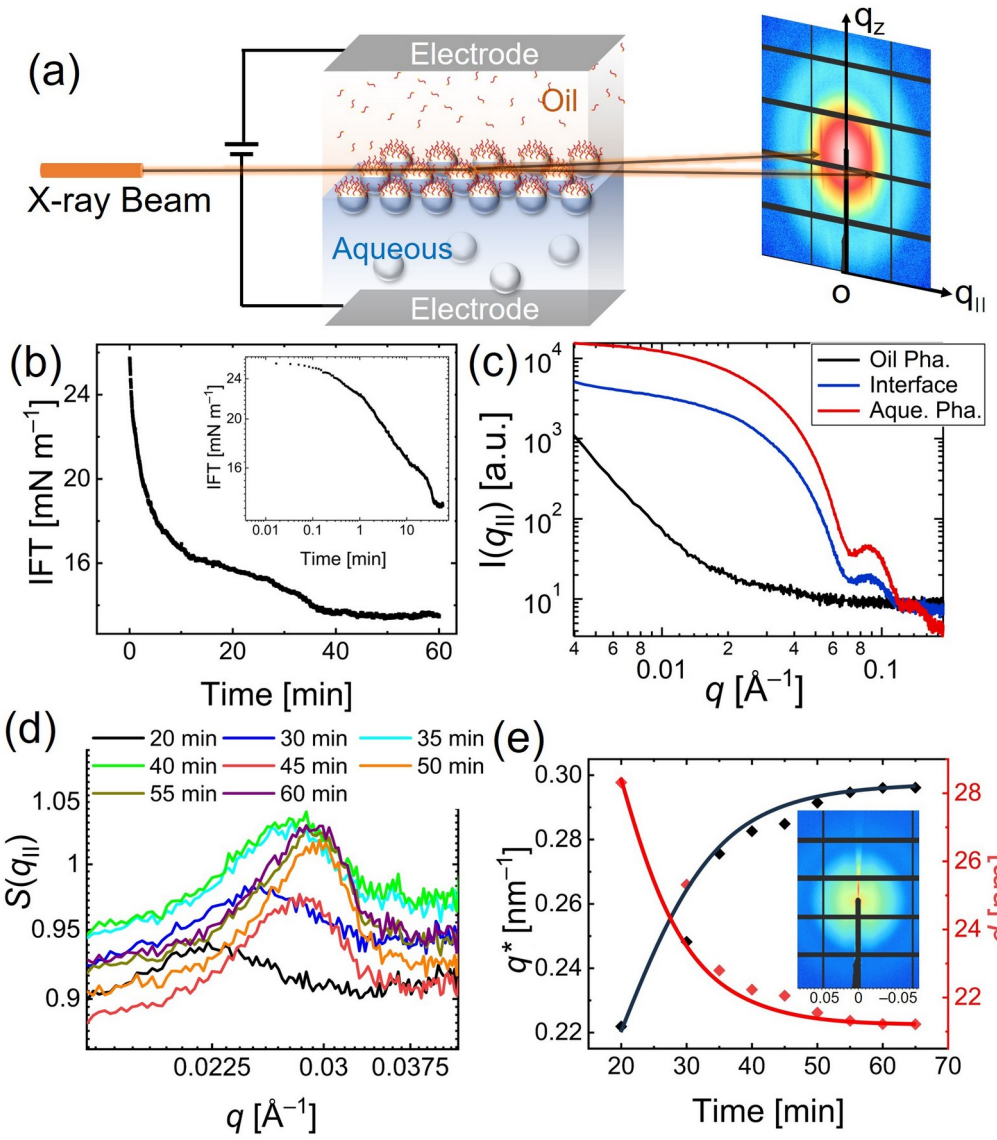

FIG 1. (a) *In-situ* X-ray scattering experiments on NPS assemblies at the water/oil bilayer interface while subjected to an external electric field. (b) Interfacial tension IFT vs interface aging time measured by the pendant drop tensiometry under no field. The concentration of Au NPs is 3.6 nM and that of the PS-triNH$_2$ is 1 mg mL^{-1}. (c) 1D X-ray scattering spectra of bulk oil, bulk Au NPs phase and interfacial region of a water/toluene bilayer. (d) Time evolution of the structure factor, $S(q)$, of the bilayer interface packed Au NPSs monolayer at different aging time without an electric field. (e) The relationship between the mean peak position, q^*, and center-to-center interparticle distance, d, between the NPSs with time. The inset shows the 2D X-ray scattering signal obtained from an interface laden with Au NPs after aging for 20 min.

Fig. 1(a) illustrates the *in-situ* X-ray scattering measurements on a dense assembly of spherical Au NPs at a water/toluene bilayer interface with/without an external electric field. A planar interface is prepared between an aqueous dispersion of carboxyl-functionalized Au NPs and a toluene solution of ω-(diethylene triamine)-terminated polystyrene (PS-triNH$_2$) that is used to facilitate the adsorption of the NPs to the interface. PS-triNH$_2$ possesses

several pKa values, approximately at 4, 7.5, and 10, attributable to its triamine structure, and the carboxylic acid-functionalized Au NPs display a pKa value at approximately 5. At a neutral pH of 7, the majority of the carboxylic acids on the surface of the NPs are deprotonated, rendering the NPs strongly negatively charged (Fig. S1). Surfactant molecules spontaneously adsorb to the interface to reduce the interfacial tension (IFT) (Fig. S2), which shows an increase as the pH rises due to the reduced protonation at higher pH levels. Concurrently, the amine groups within the ligand become protonated upon contact with the interface, leading to the acquisition of a positive charge. The strong electrostatic interactions between the negatively charged Au NPs and the cationic surfactant, PS-triNH_2, leads to a substantial enhancement in the binding energy per NP by anchoring the NPs to the absorbed ligands at the interface, which facilitates the densification of the assembly and reduces the IFT substantially (Fig. 1(b) and Figs. S2–S3). All the IFT data mentioned in this paper is measured by the pendant drop tensiometry.

Absent an external field, it is observed that the IFT of the interface decorated with NPSs is gradually decrease with time, and the change in the IFT should be directly related to the packing density of the NPSs at the interface. The IFT initially shows a rapid decrease (<12 min), as the NPSs form and assemble at the interface. It then shows a more gradual decrease (12–28 min), as more NPSs form and assemble at the interface, where the amount of space remaining at the interface is reduced and the adsorption is slowed. Further reorganization of the NPSs at the interface due to interparticle interactions, e.g., capillary forces[54-56], that densifies the assembly further give rise to the step decrease in the IFT (~30 min), after which the IFT plateaus at a value of ~13.5 mN m^{-1}. The balance between electrostatic repulsion and capillary attraction among the NPSs establishes the equilibrium distance between particles.

During the *in-situ* scattering measurement, as the X-ray beam is scanned vertically from the toluene to water phases, the interface is located from a sharp decrease in the transmitted intensity. To be noted that the scattering experiments were not performed on a pendant drop due to the absorption of the X-rays, but at the interface between an oil/water bilayer. Attempts were made to replicate the conditions of the pendant drop studies. The Au NPs dispersed in the aqueous phase are first characterized by X-ray scattering, as shown in Fig. S4. The dispersion of NPs in the aqueous phase shows a series of maxima as a function of the scattering vector, $q = (4\pi/\lambda) \sin \theta$, where 2θ is the scattering angle and λ is the wavelength, characteristic of the sphere scattering function, while the scattering from the toluene solution of the PS-triNH_2 ligands monotonically decreases as a function of q, as would be expected. The scattering from the interfacial region, while closely resembling the scattering from the aqueous dispersion of NPs, shows some distinct differences (Fig. 1(c)). Here, the incident X-ray beam, ~0.5 mm in diameter, intercepts not only the assembly of NPs at the interface, but also the liquid

phases above and below the interface. Even though the thickness of the NPSs assembly is small in comparison to the beam diameter, the areal density of the NPSs is orders of magnitude higher than the number of NPs in the dispersion intercepted by the beam (Fig. S5). The in-plane scattering, $I(q)$, can reasonably be treated as the product of the form factor $P(q)$, characteristic of the NP size and shape, and structure factor $S(q)$, characteristic of the in-plane packing of the NPSs. The scattering from NP dispersion in the aqueous phase gives $P(q)$. Therefore, the structure factor of the NPS assembly at the interface can be well approximated by $S(q) = I(q)/P(q)$[57].

$S(q)$ for the in-plane scattering of the assembly of NPSs at the interface is shown in Fig. 1(d) as a function of time. A distinct maximum in $S(q)$ is evident, characteristic of the average center-to-center distance d between the NPSs. The peak position, q^*, shifts to higher q over time, corresponding to a decrease in the center-to-center distance from 28.3 nm to 21.5 nm, as shown in Fig. 1(e). The progressive increase in the integrated area and decrease in the full width at half maximum under the interference maximum signify an increase in the number of NPS assembled at the interface and an enhancement in the in-plane correlations within the self-assembled NPS array (Fig. S6). After the formation and assembly of the NPSs at the interface, scattering rods are evident, characteristic of an Au NPS monolayer at the interface (inset in Fig. 1(e)). The broad size distribution of the NPs prevents the long–range structural ordering of the interfacial assembly even at high areal densities (Fig. S7). A plot of the IFT and NP interparticle distance as a function time clearly shows the close correlation between the two (Fig. S8).

The application of an electric field enables the manipulation of the packing of the NPSs at the interface, leading to an oversaturation assembly. With a negatively charged interface, the NPs are stable until the voltage is turned off, whereupon a burst of microdroplets are explosively ejected from the interface (Figs. 2(a)–(b) and Movie S1). Irregular shape microdroplets, e.g., cylindrical, triangular, and ellipsoidal, are seen under optical microscopy (Fig. S9), demonstrating that NPS assemblies on the microdroplet surfaces are jammed, preventing them from relaxing to a spherical shape[58, 59]. The number and speed of the jettisoned microdroplets increases with increasing applied voltage, due to the oversaturation of the NPSs at the interface driven by the negative potential drop across the interface. This phenomenon was previously analyzed through IFT data to indirectly infer the packing density[37], while we're trying to quantitively characterize this behavior here.

In situ small angle X-ray scattering is used to investigate the packing of the NPSs at the water/toluene bilayer interface under an applied electric field, as shown in Fig. 1(a). When subjected to an external electric field (with the aqueous phase negatively polarized), cations are moved away from the interface while the negative ions and NPs are propelled towards to the interface, leading an intensified electrostatic repulsion between the NPSs at the interface. The external field has the potential to overcome this repulsion,

thereby enhancing the density of interfacial packing. Meanwhile, the water/toluene interface becomes progressively more negatively charged, inhibiting the further approach of negatively charged NPs once the repulsion between the negatively charged interface and the NPs becomes stronger than or equal to the force exerted by the external field (Fig. S5). To be noted that an applied field also enhances the transport of uncharged PS-triNH_2 to the interface due to electrohydrodynamic flows generated on both sides of the interface[60]. Although the capillary tube and the pendant droplet exhibit different meniscus formations, the particles involved are significantly smaller in comparison. As a result, the effect of curvature can be assumed to be ignored during data analysis. As the applied external field is increased in a stepwise manner, the position of the interference maximum shifts to higher *q* (Fig. 2(c)–(d)), showing that the areal density of NPSs at the interface increases. Since the interfacial area has not changed, this result also indicates that the number of NPSs at the interface has increased. Absent an external field, the equilibrium interparticle distance is ~21.5 nm (Fig. 1), ~40% of 2D areal fraction. The high degree of deprotonation of the carboxyl ion groups at a neutral pH enhances the interparticle electrostatic repulsion and inhibits a denser packing of the NPSs (Fig. 1 and Fig. S1). However, when an electric field is applied, NPS areal density significantly increases, overcoming the interparticle repulsion, up to several tens of nN,[61] and reducing the distance between them to 16.2 nm (71%), nearly the size of a single particle (Fig. 2), which results in the accumulation of Coulombic energy within the oversaturated assemblies and rapid dissipation of the energy after removal of external field. From the 2D scattering image, Bragg rods, interference maxima extended normal to the plane of the interface) are clearly evident, which are characteristic of the monolayer nature of the NPS assembly. Although the electric field depletes the free cations at the interface and enhances the interparticle electrostatic repulsion, the external electric field is sufficiently strong to overcome these and densify the NPS packing. It's worth highlighting that the electric field strength has a significant impact on the oversaturation ratio of NPS assemblies at the interface. Notably, the q^* position remains stable even after a prolonged aging period (Fig, S5 and **Fig. S10**), but it clearly shifts to a higher *q* position under the influence of a stronger electric field. The increase in integrated peak area with increasing applied electric field also clearly reflects the increase in the number of NPSs that are strongly bound to the interface[34] (Fig. **S11**). With the anchoring of the cationic surfactants to the Au NPs, the binding energy per particle at the interface is significantly increased, suppressing any desorption of the individual NPs from the interface. However, when the field is turned off, the in-plane pressure arising from the electrostatic repulsion between the NPSs destabilizes the interface and triggers an explosive emulsification with hundreds of thousands of microdroplets coated with a monolayer of NPSs being jettisoned from the interface into the oil phase (Fig. 2b). Notably, reversing the field direction,

with a positively charged needle, does not result in this behavior and barely affects X-ray scattering, showing no additional Au NPs are drawn to the interface (Fig. **S12**).

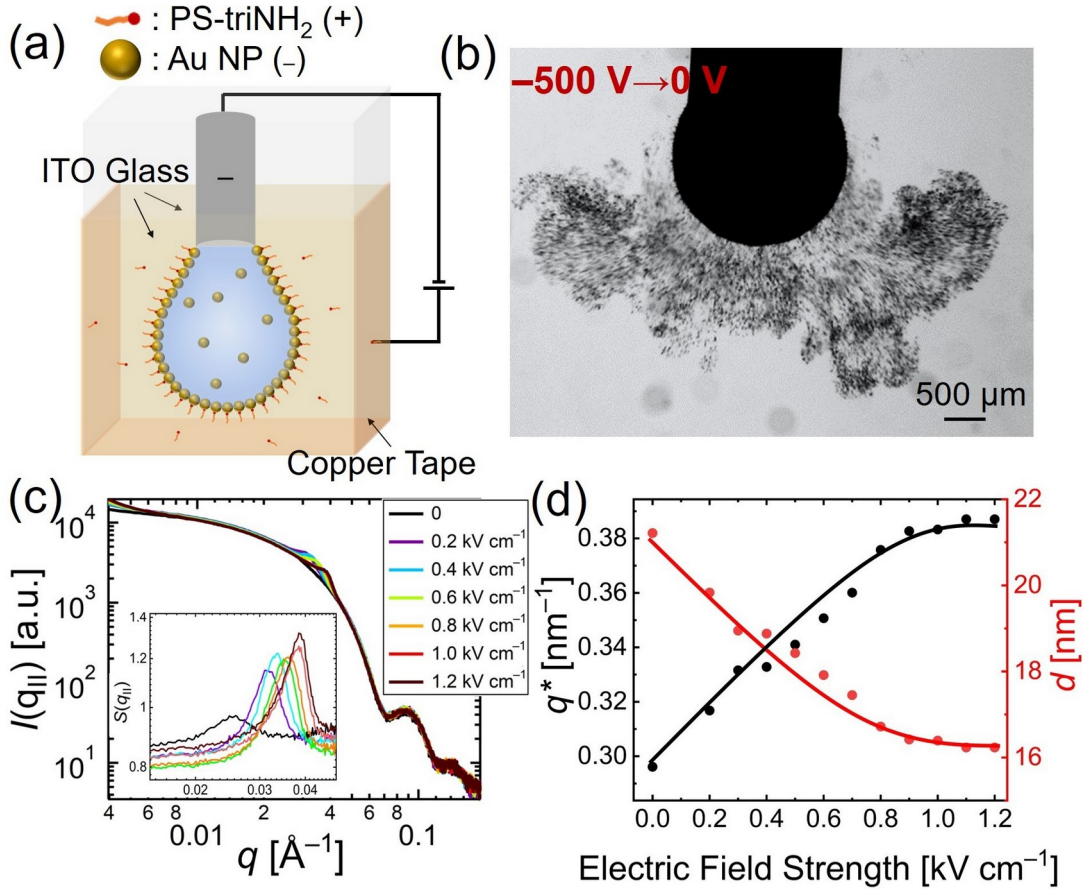

FIG. 2. (a) Schematic of the pendant droplet explosive emulsification experimental setup. (b) The optical image of the aqueous droplet (C_{Au}= 3.6 nM) immersed in a PS-triNH2 solution (1 mg mL^{-1}) in toluene after a bias voltage of –500 V applied to the needle is turned off. (c) 1D scattering profile, I(q), and S(q), of the bilayer interface packed Au NPSs monolayer, dependent on the external applied field. (d) The relationship between q^* and d with the applied electric field strength.

The degree of deprotonation of the carboxyl groups, which influences the interparticle electrostatic interactions, also alters the ability of the NPSs assemblies to store the potential energy at the interface, and depends on the pH of the aqueous phase. At lower pH values, most of the amine groups of the ligands adsorbed at the interface become protonated, granting it higher interfacial activity (Fig. S2) and strong affinity towards the negatively charged NPs. Meanwhile, for the carboxylic acid-functionalized NPs, fewer carboxyl groups are deprotonated, resulting in a lower charge density (Fig. S1). This, in turn, considerably diminishes the electrostatic repulsion between particles, and reduces the equilibrium interparticle distance. Absent an external field, at pH of 4, the equilibrium center-to-center distance is ~17 nm, reducing the IFT

to ~12.1 mN m^{-1} (Figs. 3(a)–(b)). This can be attributed to the weak electrostatic repulsion between neighboring Au NPs and the strong interfacial activity of the polystyrene surfactants that strongly anchor the NPSs to the interface. The application of an electric field only marginally enhances the packing density of the Au NPs due to their inherent tightly-packed structure. This is evident from the shift of the scattering peak to higher *q* values, ranging from 0.364 nm^{-1} to 0.389 nm^{-1}, with the interparticle distance decreasing from 17.2 nm to 16.1 nm (Fig. **S13**). The narrowing of the Bragg peak also suggests enhanced nanoparticle correlations at the interface. However, the weak electrostatic repulsion between the Au NPSs reduces the accumulated electrostatic energy at maximum packing, weakening the explosive emulsification behavior.

Under alkaline conditions (Figs. 3(c)–(d)), PS-triNH_2 maintains its interfacial activity, though the electrostatic attraction between the ligand and nanoparticles diminishes as the amine groups become less protonated. Consequently, the areal density of Au NPSs assembled at the interface is much lower, with an average interparticle distance of ~30 nm, corresponding to a higher IFT of 15.3 mN m^{-1}. In addition to the charge density of the NPs, the interfacial activity of the polymer surfactant plays an important role in generating the out-of-equilibrium system. The adsorption of cationic surfactants decreases with increasing pH due to the decreased protonation. Consequently, absent electrostatic attractions from the surfactants at the interface, the negatively charged Au NPs tend to remain dispersed in the bulk phase rather than adsorbing at the interface. Upon applying the electric field, a noticeable shift in the peak position is observed in the X-ray scattering profiles. At low electric field strength (<0.8 kV cm^{-1}), the peak position moves towards higher *q* values, and at high electric field strength (>0.8 kV cm^{-1}), the interparticle repulsion becomes stronger due to the depletion of the counterions from the interface[52], which drives the *q* back to lower values. This non-monotonic behavior is not observed under neutral/acid conditions, due to the higher interfacial activity of the cationic ligands that anchor to the interface with the protonation of the amine groups. To be noted that even with a medium electric field (0.4-1.0 kV cm^{-1}), the Au NPs still remain dispersed with relatively large interparticle distances for those NPSs formed at the interface, ~27 nm, that minimizes the interparticle interactions. As a result, while the high degree of deprotonation of the carboxyl group does enhance the interparticle repulsion in an alkaline solution, the large interparticle distances for those NPSs formed at the interface reduces the interparticle interactions even under the field (Fig. **S13**), weakening the explosive behavior.

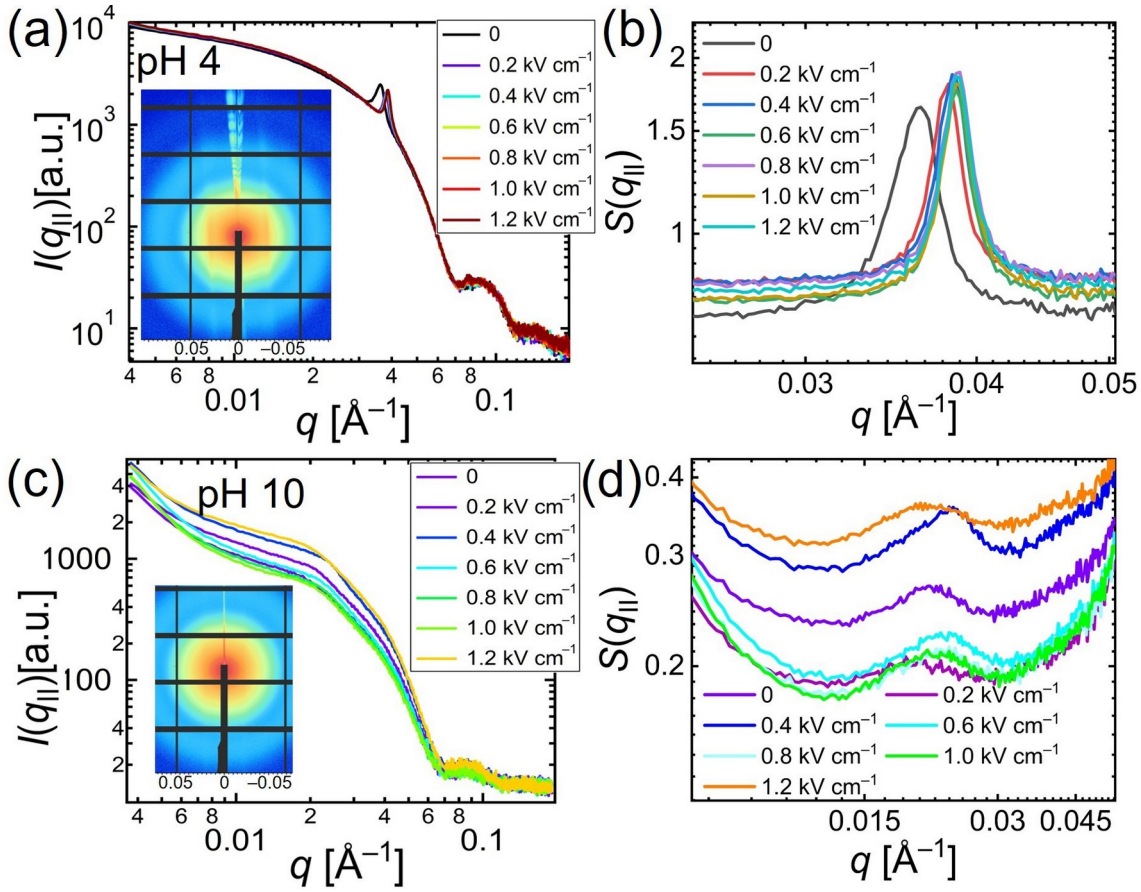

FIG. 3. (a) $I(q)$ and, (b) $S(q)$, of the NP-laden interface between water/toluene bilayer at pH of 4 varying with the electric field strength. (c) $I(q)$, and (d) $S(q)$, of the NP-laden interface between water/toluene bilayer and at pH of 10 varying with the electric field strength. The inset the 2D X-ray scattering signal of the interface.

At high ligand concentration, well above the critical micelle concentration, spontaneous emulsification occurs, limiting the areal density of the Au NPs at the interface. Spontaneous emulsification begins at ~10.5 mN m^{-1}, after an aging time of 30 s, (Fig. 4(a)). Consequently, while the adsorption of the cationic ligand weakens the electrostatic repulsion, the interparticle distance is limited to 21.8 nm due to the spontaneous emulsification (Fig. 4(b)). Under the influence of the electric field, a shift towards higher q values is still observed, reducing the interparticle distance to 20.8 nm, which is a curious result due to the fact that both the number of NPs and also the area of the parent droplet are decreasing during spontaneous emulsification (Fig. **S14**).

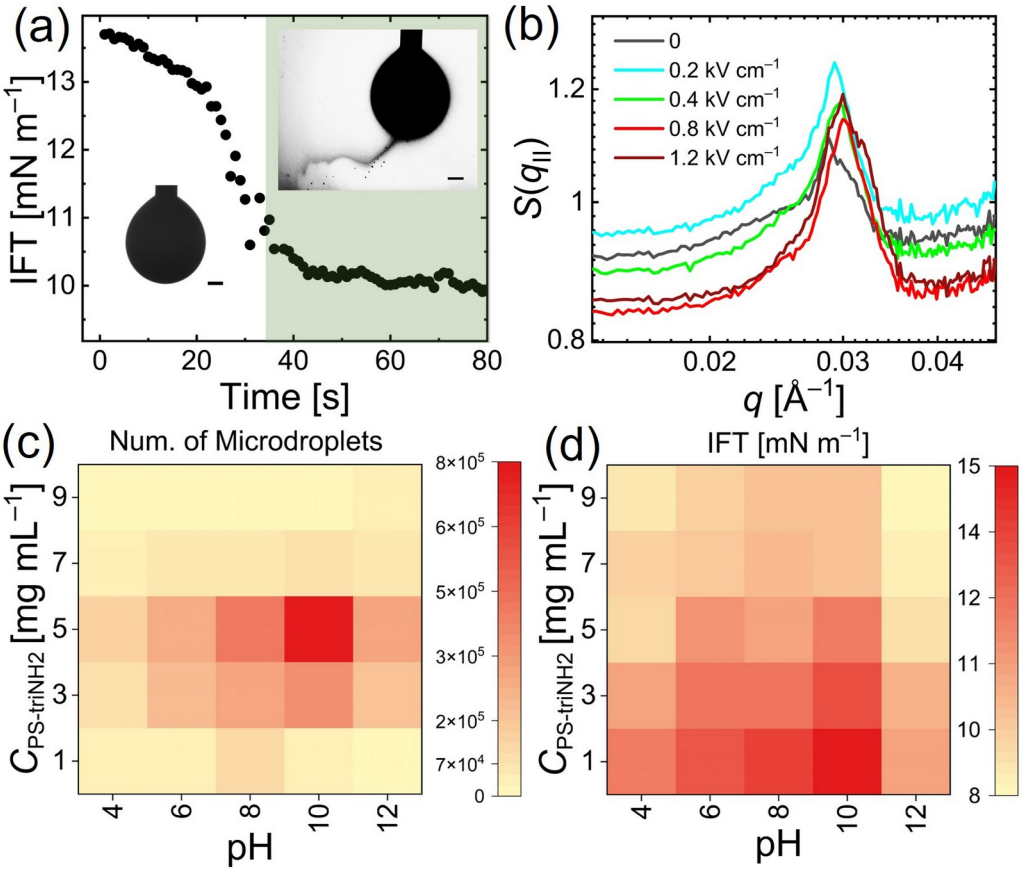

FIG. 4. (a) Time evolution of the IFT at high ligand concentration of 10 mg mL^{-1} measured by the pendant drop tensiometry. The inset image at the clear area displays the optical image of the pendant aqueous droplet immediately after immersion into the toluene phase, and that at the shaded green area reveals the droplet undergoing spontaneous emulsification. Scale bar: 500 μm. (b) $S(q)$ of the NP-laden interface between water/toluene bilayer, dependence on the external applied field, at pH 7 and a ligand concentration of 10 mg mL^{-1}. (c) The dependence of the total number of the microdroplets jettisoned from a pendant droplet during the explosive emulsification on both pH and ligand concentration. (d) The dependence of the IFT value on both pH and ligand concentration measured by the pendant drop tensiometry.

As previously mentioned, the efficient generation of an out-of-equilibrium system depends on the physiochemical conditions, such as pH and component concentrations. We quantified the intensity of explosive emulsification formed at different pH and ligand concentrations (Fig. 4(c)). The largest number of microdroplets jettisoned from the interface during explosive emulsification occurs at pH 10 and a ligand concentration of 5 mg mL^{-1}. However, as the ligand concentration is decreased below this, the pH associated with the maximum microdroplet formation gradually shifts towards neutral conditions. Thus, explosive emulsification depends on the interplay between interparticle interactions and the areal density. As the ligand concentration increases, more Au NPs adsorb to the interface, and form NPSs.

This interaction weakens the electrostatic repulsion, leading to a weakening of the explosive behavior. To compensate, the pH must be increased to mitigate the adsorption of the ligands, thereby enhancing interparticle repulsion. By doing so, the system is tuned to promote explosive emulsification.

Based on the IFT data (Fig. 4(d)), a very low IFT is not required to induce out-of-equilibrium behavior. On the contrary, the most intense explosive emulsification at each concentration typically takes place at relatively high IFTs, since the interface can accommodate a larger number of the excess NPs from the bulk phase and store more potential energy. It is important, though, that the Au NPSs not be too far apart to enhance the interparticle interactions. Titration studies indicate that each individual NP bears ~200 carboxyl groups. Consequently, even a minor reduction in the interparticle distance, for example, from 22 nm to 17 nm, can cause the potential energy to increase by 10^{-5} J, sufficient to offset the energy needed to expand the interface and to propel the microdroplets away from the interface at high speeds. Nevertheless, beyond a concentration of 5 mg mL^{-1}, spontaneous emulsification occurs, due to micelle solubilization[62]. This leads to a weakening of the explosive emulsification and prevents any further decrease in IFT with increasing ligand concentration.

Collectively, we conclude that by adopting X-ray scattering method, *in-situ* characterization of interfacial assembly microstructure with and without an applied field is realized quantitatively, and further, our results indicate that the electric field can store Coulombic energy at immiscible liquid/liquid interfaces by oversaturating the packing of charged NPSs. Physicochemical conditions, e.g., pH and ligand concentration, can modify the binding energy of NPSs to the interface, markedly influencing the explosive behavior. Higher ligand concentrations enhance explosive emulsification under alkaline conditions more significantly, but beyond a threshold concentration, spontaneous emulsification dominates, limiting NPSs densification under the field. This research highlights the intricate balance of factors that influence out-of-equilibrium assemblies at interfaces, and also emphasizes the importance of tailoring physicochemical conditions to achieve precise control over explosive emulsification behavior, which guides further research towards achieving controllable explosive emulsification and designing an active droplet system tailored to specific needs. This process of explosive emulsification reveals that the liquid/liquid interface acts as a dynamic reservoir, storing energy by accumulating an oversaturated layer of charged NPSs, showcasing its vast potential for applications in self-propulsion systems[37] and remotely operated soft microrobots.

This work was supported by the U.S. Department of Energy, Office of Science,

Office of Basic Energy Sciences, Materials Sciences and Engineering Division under Contract No. DE-AC02-05-CH11231 within the Adaptive Interfacial Assemblies Towards Structuring Liquids program (KCTR16). Beamline 7.3.3 of the Advanced Light Source is supported by the Director of the Office of Science, Office of Basic Energy Sciences, of the U.S. Department of Energy under Contract No. DE-AC02-05CH11231.

Reference

[1] Grzybowski, B.A., Fitzner, K., Paczesny, J., Granick, S. From dynamic self-assembly to networked chemical systems. *Chem. Soc. Rev.* 2017, 46, 5647–5678.

[2] Babu, D., Katsonis, N., Lancia, F., Plamont, R., Ryabchun, A. Motile behaviour of droplets in lipid systems. *Nat. Rev. Chem.* 2022, 6, 377–388.

[3] Klajn, R., Bishop, K.J., Grzybowski, B.A. Light-controlled self-assembly of reversible and irreversible nanoparticle suprastructures. *Proceedings of the National Academy of Sciences of the United States of America* 2007, 104, 10305-9.

[4] Erb, R.M., Son, H.S., Samanta, B., Rotello, V.M., Yellen, B.B. Magnetic assembly of colloidal superstructures with multipole symmetry. *Nature* 2009, 457, 999-1002.

[5] Whitesides, G.M., Grzybowski, B. Self-Assembly at All Scales. *Science* 2002, 295, 2418-2421.

[6] Fang, X., Kruse, K., Lu, T., Wang, J. Nonequilibrium physics in biology. *Reviews of Modern Physics* 2019, 91.

[7] Pollard, T.D., Borisy, G.G. Cellular Motility Driven by Assembly and Disassembly of Actin Filaments. *Cell* 2003, 112, 453-465.

[8] Li, M., Li, D. Redistribution of charged aluminum nanoparticles on oil droplets in water in response to applied electrical field. *Journal of Nanoparticle Research* 2016, 18.

[9] Bharti, B., Velev, O.D. Assembly of Reconfigurable Colloidal Structures by Multidirectional Field-Induced Interactions. *Langmuir : the ACS journal of surfaces and colloids* 2015, 31, 7897-908.

[10]Harraq, A.A., Choudhury, B.D., Bharti, B. Field-Induced Assembly and Propulsion of Colloids. *Langmuir : the ACS journal of surfaces and colloids* 2022, 38, 3001–3016.

[11]Dommersnes, P., Rozynek, Z., Mikkelsen, A., Castberg, R., Kjerstad, K., Hersvik, K., Otto Fossum, J. Active structuring of colloidal armour on liquid drops. *Nature communications* 2013, 4, 2066.

[12]Snezhko, A., Aranson, I.S. Magnetic manipulation of self-assembled colloidal asters. *Nature materials* 2011, 10, 698-703.

[13]Kokot, G., Piet, D., Whitesides, G.M., Aranson, I.S., Snezhko, A. Emergence of reconfigurable wires and spinners via dynamic self-assembly. *Scientific reports* 2015, 5, 9528.

[14]Aragones, J.L., Steimel, J.P., Alexander-Katz, A. Aggregation dynamics of active rotating particles in dense passive media. *Soft Matter* 2019, 15, 3929-3937.

[15]Manna, D., Udayabhaskararao, T., Zhao, H., Klajn, R. Orthogonal light-induced self-assembly of nanoparticles using differently substituted azobenzenes. *Angew Chem Int Ed Engl* 2015, 54, 12394-7.

[16]Lee, J.W., Klajn, R. Dual-responsive nanoparticles that aggregate under the simultaneous action of light and CO2. *Chemical communications* 2015, 51, 2036-9.

[17]Wang, W., Duan, W., Sen, A., Mallouk, T.E. Catalytically powered dynamic assembly of rod-shaped nanomotors and passive tracer particles. *PNAS* 2013, 110, 17744–17749.

[18]Lee, W., Amini, H., Stone, H.A., , a.D.D.C. Dynamic self-assembly and control of microfluidic

particle crystals. *PNAS* 2010, 107, 22413–22418.

[19]Song, H., Chen, D.L., Ismagilov, R.F. Reactions in droplets in microfluidic channels. *Angew Chem Int Ed Engl* 2006, 45, 7336-56.

[20]Utada, A.S., Lorenceau, E., Link, D.R., Kaplan, P.D., Stone, H.A., Weitz, D.A. Monodisperse Double Emulsions Generated from a Microcapillary Device. *Science* 2005, 308, 537-541.

[21]Cui, M., Emrick, T., Russell, T.P. Stabilizing liquid drops in nonequilibrium shapes by the interfacial jamming of nanoparticles. *Science* 2013, 25, 460-463.

[22]Liu, X., Kent, N., Ceballos, A., Streubel, R., Jiang, Y., Chai, Y., Kim, P.Y., Forth, J., Hellman, F., Shi, S., Wang, D., Helms, B.A., Ashby, P.D., Fischer, P., Russell, T.P. Reconfigurable ferromagnetic liquid droplets. *Science* 2019, 365, 264–267.

[23]Velleman, L., Sikdar, D., Turek, V.A., Kucernak, A.R., Roser, S.J., Kornyshev, A.A., Edel, J.B. Tuneable 2D self-assembly of plasmonic nanoparticles at liquid|liquid interfaces. *Nanoscale* 2016, 8, 19229-19241.

[24]Park, Y.-K., Yoo, S.-H., Park, S. Assembly of Highly Ordered Nanoparticle Monolayers at a Water/Hexane Interface. *Langmuir : the ACS journal of surfaces and colloids* 2007, 23, 10505-10510.

[25]Jia, H., Zhang, Y.F., Zhang, C., Ouyang, M., Du, S. Ligand-Ligand-Interaction-Dominated Self-Assembly of Gold Nanoparticles at the Oil/Water Interface: An Atomic-Scale Simulation. *The journal of physical chemistry. B* 2023, 127, 2258-2266.

[26]Song, L., Xu, B.B., Cheng, Q., Wang, X., Luo, X., Chen, X., Chen, T., Huang, Y. Instant interfacial self-assembly for homogeneous nanoparticle monolayer enabled conformal "lift-on" thin film technology. *Sci. Adv.* 2021, 7, eabk2852.

[27]Kim, P.Y., Fink, Z., Zhang, Q., Dufresne, E.M., Narayanan, S., Russell, T.P. Relaxation and Aging of Nanosphere Assemblies at a Water-Oil Interface. *ACS nano* 2022.

[28]Chai, Y., Lukito, A., Jiang, Y., Ashby, P.D., Russell, T.P. Fine-Tuning Nanoparticle Packing at Water-Oil Interfaces Using Ionic Strength. *Nano Lett.* 2017, 17, 6453-6457.

[29]Huang, C., Sun, Z., Cui, M., Liu, F., Helms, B.A., Russell, T.P. Structured Liquids with pH-Triggered Reconfigurability. *Advanced materials* 2016, 28, 6612-8.

[30]Xu, R., Liu, T., Sun, H., Wang, B., Shi, S., Russell, T.P. Interfacial Assembly and Jamming of Polyelectrolyte Surfactants: A Simple Route To Print Liquids in Low-Viscosity Solution. *ACS applied materials & interfaces* 2020.

[31]Qian, B., Shi, S., Wang, H., Russell, T.P. Reconfigurable Liquids Stabilized by DNA Surfactants. *ACS Appl. Mater. Interfaces* 2020, 12, 13551-13557.

[32]Su, B., Abid, J.-P., Fermin, D.J., Girault, H.H., Hoffmannova, H., Krtil, P., Samec, Z. Reversible Voltage-Induced Assembly of Au Nanoparticles at Liquid|Liquid Interfaces. *J. Am. Chem. Soc.* 2004, 126, 915–919.

[33]Montelongo, Y., Sikdar, D., Ma, Y., McIntosh, A.J.S., Velleman, L., Kucernak, A.R., Edel, J.B., Kornyshev, A.A. Electrotunable nanoplasmonic liquid mirror. *Nature materials* 2017, 16, 1127-1135.

[34]Flatté, M.E., Kornyshev, A.A., Urbakh, M. Understanding voltage-induced localization of nanoparticles at a liquid–liquid interface. *J. Phys.: Condens. Matter* 2008, 20, 073102.

[35]Boker, A., He, J., Emrick, T., Russell, T.P. Self-assembly of nanoparticles at interfaces. *Soft Matter* 2007, 3, 1231-1248.

[36]Wu, X., Bordia, G., Streubel, R., Hasnain, J., Pedroso, C.C.S., Cohen, B.E., Rad, B., Ashby, P., Omar, A.K., Geissler, P.L., Wang, D., Xue, H., Wang, J., Russell, T.P. Ballistic Ejection of Microdroplets from Overpacked Interfacial Assemblies. *Adv. Funct. Mater.* 2023, 33, 2213844.

[37]Wu, X., Xue, H., Bordia, G., Fink, Z., Kim, P.Y., Streubel, R., Han, J., Helms, B.A., Ashby, P., Omar, A.K., Russell, T.P. Self-Propulsion by Directed Explosive Emulsification. *(unpublished)*.
[38]Yang, R., Mei, L., Fan, Y., Zhang, Q., Liao, H.G., Yang, J., Li, J., Zeng, Z. Fabrication of liquid cell for in situ transmission electron microscopy of electrochemical processes. *Nature protocols* 2023, 18, 555-578.
[39]Kim, P.Y., Gao, Y., Chai, Y., Ashby, P.D., Ribbe, A.E., Hoagland, D.A., Russell, T.P. Assessing Pair Interaction Potentials of Nanoparticles on Liquid Interfaces. *ACS nano* 2019, 13, 3075-3082.
[40]Kim, P.Y., Gao, Y., Fink, Z., Ribbe, A.E., Hoagland, D.A., Russell, T.P. Dynamic Reconfiguration of Compressed 2D Nanoparticle Monolayers. *ACS nano* 2022, 16, 5496-5506.
[41]Pienpinijtham, P., Han, X.X., Ekgasit, S., Ozaki, Y. An ionic surfactant-mediated Langmuir-Blodgett method to construct gold nanoparticle films for surface-enhanced Raman scattering. *Physical chemistry chemical physics : PCCP* 2012, 14, 10132-9.
[42]Cecchini, M.P., Turek, V.A., Demetriadou, A., Britovsek, G., Welton, T., Kornyshev, A.A., Wilton-Ely, J.D.E.T., Edel, J.B. Heavy Metal Sensing Using Self‐Assembled Nanoparticles at a Liquid–Liquid Interface. *Advanced Optical Materials* 2014, 2, 966-977.
[43]Tian, H., Li, H., Fang, Y. Binary Thiol-Capped Gold Nanoparticle Monolayer Films for Quantitative Surface-Enhanced Raman Scattering Analysis. *ACS applied materials & interfaces* 2019, 11, 16207-16213.
[44]Bramhaiah, K., John, N.S. Hybrid films of reduced graphene oxide with noble metal nanoparticles generated at a liquid/liquid interface for applications in catalysis. *RSC Advances* 2013, 3, 7765.
[45]Kim, K., Han, H.S., Choi, I., Lee, C., Hong, S., Suh, S.H., Lee, L.P., Kang, T. Interfacial liquid-state surface-enhanced Raman spectroscopy. *Nature communications* 2013, 4, 2182.
[46]Jain, P.K., Huang, W., El-Sayed*, M.A. On the Universal Scaling Behavior of the Distance Decay of Plasmon Coupling in Metal Nanoparticle Pairs: A Plasmon Ruler Equation. *Nano letters* 2007, 7, 2080-2088.
[47]Turek, V.A., Cecchini, M.P., Paget, J., Kucernak, A.R., Kornyshev, A.A., Edel, J.B. Plasmonic Ruler at the Liquid-Liquid Interface. *ACS nano* 2012, 6, 7789–7799.
[48]Fink, Z., Wu, X., Kim, P.Y., McGlasson, A., Abdelsamie, M., Emrick, T., Sutter-Fella, C.M., Ashby, P.D., Helms, B.A., Russell, T.P. Mixed Nanosphere Assemblies at a Liquid-Liquid Interface. *Small* 2023, e2308560.
[49]Hu, J., Spotte-Smith, E.W.C., Pan, B., Garcia, R.J., Colosqui, C., Herman, I.P. Spatiotemporal Study of Iron Oxide Nanoparticle Monolayer Formation at Liquid/Liquid Interfaces by Using In Situ Small-Angle X-ray Scattering. *The Journal of Physical Chemistry C* 2020, 124, 23949-23963.
[50]Paracini, N., Gutfreund, P., Welbourn, R., Gonzalez-Martinez, J.F., Zhu, K., Miao, Y., Yepuri, N., Darwish, T.A., Garvey, C., Waldie, S., Larsson, J., Wolff, M., Cardenas, M. Structural Characterization of Nanoparticle-Supported Lipid Bilayer Arrays by Grazing Incidence X-ray and Neutron Scattering. *ACS applied materials & interfaces* 2023, 15, 3772-3780.
[51]Li, H., Roth, S.V., Freychet, G., Zhernenkov, M., Asta, N., Wagberg, L., Pettersson, T. Structure Development of the Interphase between Drying Cellulose Materials Revealed by In Situ Grazing-Incidence Small-Angle X-ray Scattering. *Biomacromolecules* 2021, 22, 4274-4283.
[52]Bera, M.K., Chan, H., Moyano, D.F., Yu, H., Tatur, S., Amoanu, D., Bu, W., Rotello, V.M., Meron, M., Kral, P., Lin, B., Schlossman, M.L. Interfacial localization and voltage-tunable arrays of charged nanoparticles. *Nano letters* 2014, 14, 6816-22.
[53]Wu, L., Wang, X., Wang, G., Chen, G. In situ X-ray scattering observation of two-dimensional

interfacial colloidal crystallization. *Nature communications* 2018, 9, 1335.

[54]Garbin, V., Crocker, J.C., Stebe, K.J. Nanoparticles at fluid interfaces: exploiting capping ligands to control adsorption, stability and dynamics. *Journal of colloid and interface science* 2012, 387, 1-11.

[55]Cheng, Q., Fang, H., Cao, R., Ma, Z., Wang, S., Xie, R., Xia, H., Wang, D. Interfacial self-assembly of nanoparticles into macroscopic, monolayered films. *Supramolecular Materials* 2022, 1, 100021.

[56]Nikolaides, M.G., Bausch, A.R., Hsu, M.F., Dinsmore, A.D., Brenner, M.P., Gay, C., Weitz, D.A. Electric-field-induced capillary attraction between like-charged particles at liquid interfaces. *Nature* 2002, 420, 299-301.

[57]Li, T., Senesi, A.J., Lee, B. Small Angle X-ray Scattering for Nanoparticle Research. *Chemical reviews* 2016, 116, 11128-80.

[58]Cui, M., Emrick, T., Russell, T.P. Stabilizing liquid drops in nonequilibrium shapes by the interfacial jamming of nanoparticles. *Science* 2013, 25, 460–463.

[59]Forth, J., Kim, P.Y., Xie, G., Liu, X., Helms, B.A., Russell, T.P. Building Reconfigurable Devices Using Complex Liquid-Fluid Interfaces. *Adv. Mater.* 2019, 31, e1806370.

[60]Mhatre, S., Simon, S., Sjoblom, J. Experimental Evidence of Enhanced Adsorption Dynamics at Liquid-Liquid Interfaces under an Electric Field. *Anal. Chem.* 2020, 92, 12860–12870.

[61]Liu, Q., Sun, Z., Santamarina, J.C. Self-assembled nanoparticle-coated interfaces: Capillary pressure, shell formation and buckling. *Journal of colloid and interface science* 2021, 581, 251-261.

[62]Meredith, C.H., Moerman, P.G., Groenewold, J., Chiu, Y.J., Kegel, W.K., van Blaaderen, A., Zarzar, L.D. Predator-prey interactions between droplets driven by non-reciprocal oil exchange. *Nature chemistry* 2020, 12, 1136-1142.